Tropical Convection and Precipitation Regimes in the Western United States

KINGTSE C. MO AND R. W. HIGGINS

Climate Prediction Center, NCEP/NWS/NOAA, Washington, D.C.

(Manuscript received 28 May 1997, in final form 18 September 1997)

ABSTRACT

The authors have documented the relationship between tropical convection and precipitation regimes in the western United States. Circulation patterns associated with precipitation regimes are described and physical mechanisms are proposed. Contributions from intraseasonal and interannual bands are examined.

When enhanced convection is located in the western Pacific, dry conditions in the Southwest (SW) and wet conditions in the Pacific Northwest (PNW) are observed. Fluctuations in both intraseasonal and interannual bands contribute to the rainfall variability. Enhanced convection in the western Pacific is accompanied by suppressed convection in the central Pacific. The associated Rossby wave vorticity source (S) anomalies keep the Pacific jet west of 150°W. A westward shift of the storm track to the North Pacific also contributes to dry conditions in the SW and wetness in the PNW. When enhanced tropical convection is located near 150°E, substantial contributions to outgoing longwave radiation anomalies are from fluctuations in the intraseasonal band. A wave train extends from the convective area in the Tropics to North America, where negative 200-hPa streamfunction anomalies are consistent with wetness in California and dry conditions in the PNW.

When tropical convection is enhanced in the central Pacific from the date line to 135°W, most contributions are from the interannual band. The positive S anomalies associated with an enhanced local Hadley cell extending from the North Pacific to California are responsible in part for the eastward shift of the subtropical jet. The storm track moves southeast and is consistent with wet conditions in the SW.

1. Introduction

Precipitation in the western United States has been linked to tropical convection at both interannual (IA) and intraseasonal (IS) timescales. At interannual timescales, previous studies (Schonher and Nicholson 1989; Cayan and Peterson 1989; Cayan and Webb 1992; Redmond and Cayan 1994) have indicated that at least a portion of precipitation variability in the western United States is related to El Niño–Southern Oscillation (ENSO) during the winter season. Warm events are associated with relatively dry and warm conditions in the Pacific Northwest (PNW) and wet and cold conditions in the Southwest (SW) during winter. Cold events favor wet and cold conditions in the PNW and dry and warm conditions in the SW. Figure 1 plots the observed mean (December–March) winter precipitation over Southern California (32°–38°N, 118°–125°W) with the winter mean removed (Fig. 1a) and the standalized Tahiti–Darwin Southern Oscillation index (SOI) (Fig. 1b). Below normal precipitation over Southern California was found during cold ENSO events (1971, 1976, and 1989) indicated by the positive SOI values and above normal precipitation was favored during warm ENSO events (1969, 1973, 1978, and 1983) indicated by negative SOI values. However, there are many exceptions. For example, precipitation was below normal during the 1987 warm event and was above normal during 1980, which was not classified as a warm ENSO event.

In addition to ENSO, precipitation in California is also moderated by the tropical intraseasonal oscillation (IO) and local influences. Based on persistent rainfall events in California, Mo and Higgins (1998) found that wet episodes in the SW are favored when enhanced convection associated with the tropical IO reaches 150°E. Dry events tend to occur when enhanced convection is located at 120°E. They also found that when rainfall in the eastern Pacific just north of the equator from 10°–20°N is suppressed (enhanced), the SW is more likely to receive above (below) normal rainfall. It is clear that tropical heating at all timescales and at different tropical locations influences precipitation over the western region.

Many previous studies have used monthly mean precipitation or the outgoing longwave radiation (OLR) as a proxy for rainfall. However, monthly mean data cannot describe precipitation associated with the tropical IO. In midlatitudes, an OLR anomaly may not be a good indicator for rainfall. Since rainfall over the western United States is influenced by both remote and local forcing, it is important to know whether or not precip-

Corresponding author address: Kingtse C. Mo, Climate Prediction Center, NCEP/NWS/NOAA, W/NP52, 4700 Silver Hill Rd., Stop 9910, Washington, DC 20233-9910.
E-mail: wd52km@sgi44.wwb.noaa.gov

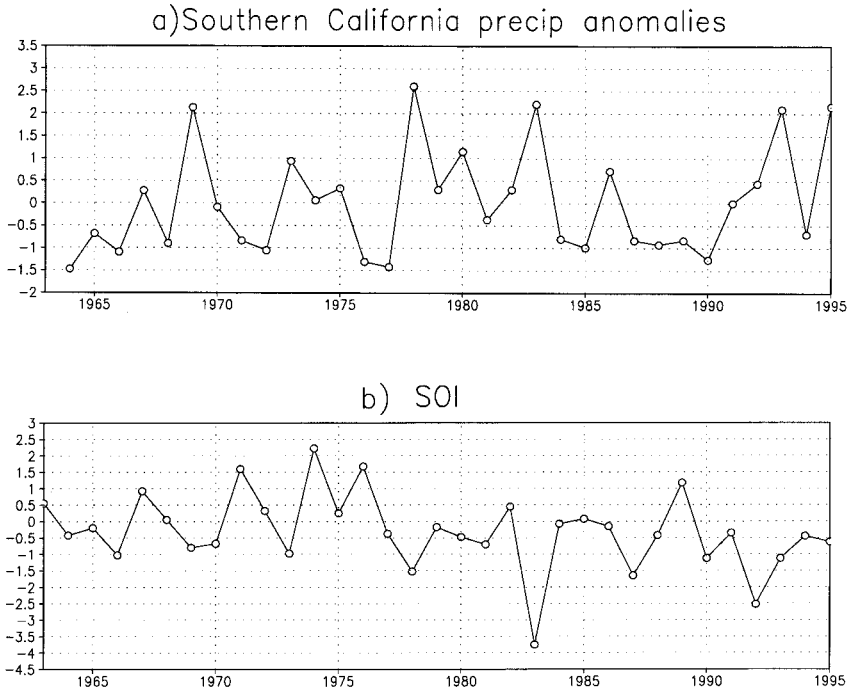

FIG. 1. (a) Observed winter (December–March) precipitation mean anomalies averaged over Southern California (32°–38°N, 118°–125°W) in mm day^{-1}, and (b) the winter mean SOI with anomalies normalized by the mean annual standard deviation.

itation is sensitive to the exact location of tropical convection.

This study capitalizes on a recently compiled multiyear (1963–95) hourly precipitation database (Higgins et al. 1996) and the National Centers for Environmental Prediction–National Center for Atmospheric Research (NCEP–NCAR) reanalysis data (Kalnay et al. 1996) to examine the precipitation regimes in the western United States. The daily dataset is better suited for examining precipitation in the United States associated with convection at different tropical locations and it allows us to separate contributions from IA and IS bands. Composites of precipitation anomalies are formed by keying to OLR anomalies (OLRAs) averaged over base boxes in the Tropics. By moving the base region from the Indian Ocean to the eastern Pacific, we document the linkages between locations of tropical heating and precipitation patterns in the western United States during boreal winter.

Dettinger et al. (1998) recognized the importance of the jet stream location to precipitation in California. We adopt the one-level vorticity balance approach of Sardeshmukh and Hoskins (1988) to link tropical heating to the shift of the jet stream and discuss the impact on precipitation regimes. This approach has been used to diagnose the tropical–extratropical relationships during ENSO (Rasmusson and Mo 1993) and during the tropical IO (Berbery and Paegle 1993).

The datasets and procedures used in this study are described in section 2. The precipitation regimes and the associated convection and circulation patterns are presented in section 3. Contributions from the IS and IA bands are discussed in section 4. The lagged responses of the precipitation regimes to tropical convection are given in section 5 and physical mechanisms are examined in section 6. Conclusions are given in section 7.

2. Data and procedures

a. Data

The data used to examine the atmospheric circulation are daily mean global gridded analyses from the NCEP–NCAR reanalysis (Kalnay et al. 1996) for the period from 1973 to 1995. The data are on a 2.5° lat × 2.5° long grid with 28 levels in the vertical. Daily averages of National Oceanic and Atmospheric Administration satellite OLR are used as a proxy for tropical convection (Liebmann and Smith 1996). The OLR dataset covers the period from 1 June 1974 to 31 December 1995 with 10 months (1 March–31 December 1978) missing. The seasonal cycle at each grid point is defined as the grand mean plus the annual and semiannual cycles. Anomalies are defined as departures of daily values from the seasonal cycle. The 200-hPa streamfunction data are used to describe the atmospheric circulation because the tropical features are better represented than 500-hPa heights. The eddy–streamfunction anomalies are obtained by removing the zonal mean at each latitude. Low-pass-filtered fields (periods greater than 10 days) are obtained

by applying the low-pass filter of Blackmon (1976). Synoptic-scale eddies (periods between 2.5 and 6 days) are obtained by applying a bandpass filter (Blackmon 1976). To obtain the IS signal, the previously low-pass-filtered anomalies are filtered using the minimum bias window developed by Papoulis (1973) to retain periods in the range of 10–90 days. The IA signal with periods greater than 90 days is obtained in the same way. The western region receives most of its precipitation from December to March (Mo and Higgins 1998), which we define as the winter season.

Over the United States, daily observed precipitation derived from gridded hourly station data (Higgins et al. 1996) is used to obtain precipitation composites. The data are on a 2° lat × 2.5° long grid covering the period from 1963 to 1995. Daily precipitation anomalies are defined as departures from the mean daily values for the entire period.

b. Procedures

1) Composite

To objectively search for linkages between the precipitation patterns in the western United States and tropical heating, composites of daily OLRAs, precipitation, 200-hPa winds, and eddy–streamfunction anomalies are calculated based on OLRAs averaged over 10° × 10° base boxes in the Tropics. Five-day running means are formed from the daily precipitation before compositing. The distribution function for 5-day mean rainfall values is close to a normal distribution after a square root transformation. For a given base box, composites for the above fields are obtained when the OLR anomaly averaged over the box is below −0.8 standard deviations. Along a given latitude, there are 31 boxes from 90°E to 120°W. The latitude varies from 10°S to 10°N. On average, there are about 18% of the days (about 520 maps) in a composite for each base box in the central Pacific 160°E–160°W) and about 10% of the days in a composite for each base box located in the eastern Pacific (140°–120°W). Results are not sensitive to a reasonable variation in the threshold (from −0.7 to −1.2 standard deviations). Statistical significance of each map is assessed by assuming a normal distribution of all variables except rainfall. To estimate the degrees of freedom, the decorrelation time is estimated by computing the number of consecutive days that mean OLRAs are below −0.8 standard deviations for each base box, and then averaging over all base boxes. The decorrelation time estimated in this way is 6 days.

The daily rainfall does not follow a normal distribution. Richman and Lamb (1985) examined the rainfall patterns of 3–5-day rainfall and suggested using the square root or $\log_{10}$ transformation in analyzing rainfall data. The square root transformation (Lanzante and Harnack 1982) is used for this paper. After transformation, the 5-day running means are close to a normal distribution and the procedures described above can be used to obtain composites and assess the statistical significance. Composites for rainfall anomalies and square root rainfall anomalies have similar patterns. Even though precipitation anomalies are plotted, the statistical significance is determined using the square root rainfall anomalies (Fig. 3).

2) Rossby wave vorticity source

To examine the linkages between tropical and extratropical circulation anomalies, we used the one-level vorticity balance diagnostic approach of Sardeshmukh and Hoskins (1988). The equation can be written as

$$\frac{\partial(\zeta)}{\partial t} + \mathbf{V}_{\psi}\cdot\nabla(\zeta + f) = S + \mathbf{k}\cdot\left(\frac{\partial \mathbf{V}}{\partial p}\times\nabla\omega\right) - \omega\frac{\partial\zeta}{\partial p} + F \qquad (1)$$

and

$$S = -\nabla\cdot(\mathbf{V}_{\chi}(\zeta + f)), \qquad (2)$$

where $\mathbf{V}$ is the horizontal vector wind, ζ is the relative vorticity, ω is the vertical velocity, $\mathbf{V}_{\psi}$ is the rotational wind, and S is the effective Rossby wave vorticity source that is the sum of the stretching term and the advection of absolute vorticity by the divergent wind $\mathbf{V}_{\chi}$, and F is the friction term, which is neglected. This approach was used by Rasmusson and Mo (1993) to link circulation changes in the extratropics to tropical convection in the central Pacific during the 1987–89 ENSO cycle. The same approach has been applied to study intraseasonal interactions in the Tropics and circulation anomalies in both hemispheres (Berbery and Paegle 1993; Higgins and Mo 1997). Prior to compositing, the seasonal cycle is removed from the Rossby wave vorticity source (S) and the low-pass filter of Blackmon (1976) is applied to remove periods less than 10 days.

3. Precipitation regimes in the western United States

For reference, the climatological winter (December–March) precipitation and 200-hPa streamfunction are shown in Fig. 2. On average, the maximum of the winter mean precipitation is about 7 mm day^{-1} for the PNW and 4 mm day^{-1} for California. The climatological 200-hPa streamfunction for winter shows a trough over east Asia, a ridge near the Gulf of Alaska, and a downstream trough centered at Hudson Bay. Observed precipitation anomaly composites and corresponding OLRA composites based on tropical OLRAs averaged over 10° × 10° boxes from the western Pacific (120°E) to the eastern Pacific (120°W) at 5°S are given in Figs. 3 and 4, respectively. Figure 5 shows the 200-hPa eddy–streamfunction anomaly composites for the same base points.

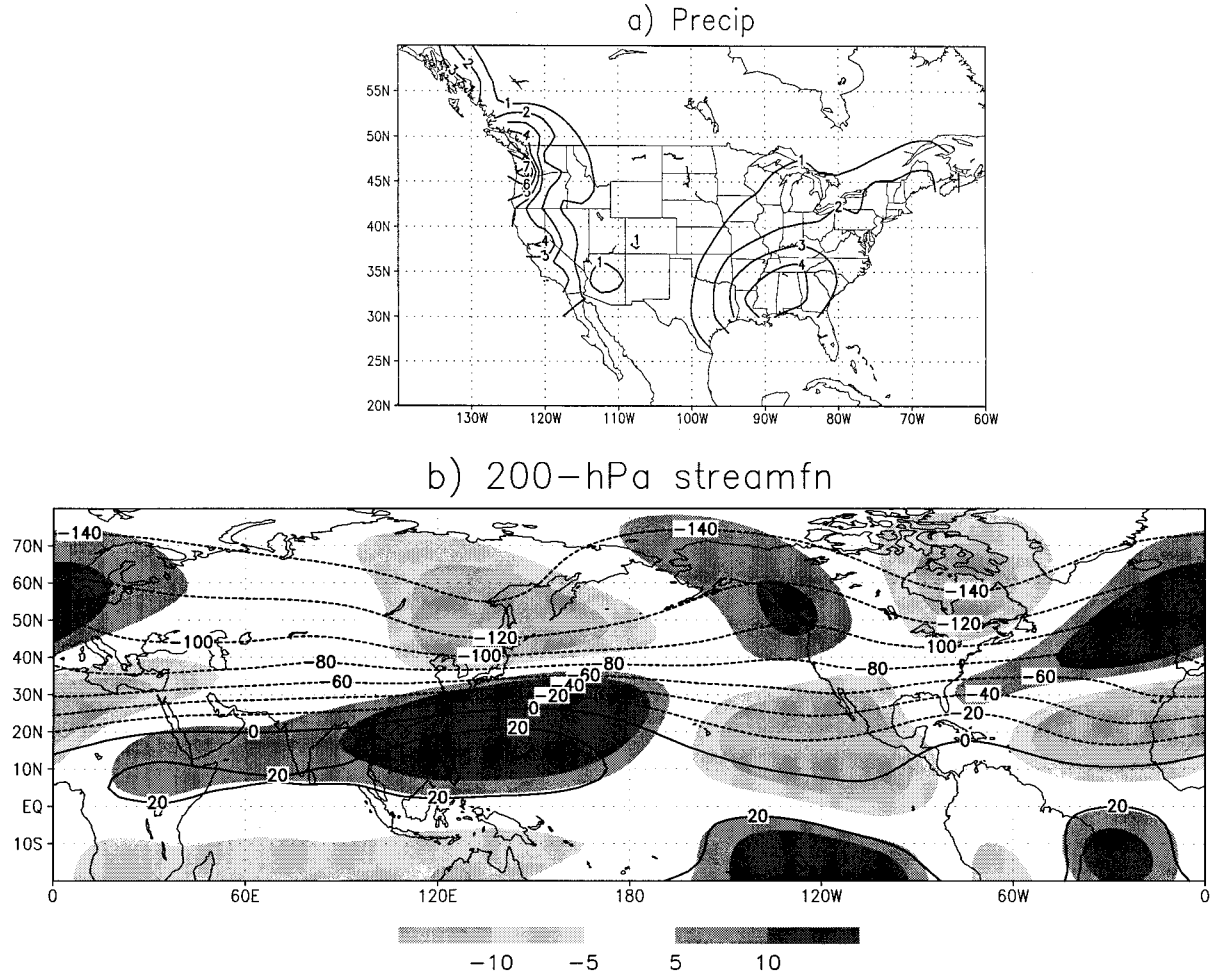

FIG. 2. (a) Mean precipitation for December–March 1963–95. Contour interval is 1 mm day^{-1}, and (b) mean 200-hPa streamfunction (contours) and eddy–streamfunction (shaded) for December–March 1974–95. Contour interval is 20 $\times$ 10^5 m^2 s^{-1}.

All OLRAs and 200-hPa eddy–streamfunction anomaly composite maps pass the field significance test.

When enhanced convection is located over the Indian Ocean (90°–100°E), the precipitation anomaly in the United States is not significant at the 95% level. When enhanced convection is centered in the western Pacific (110°–130°E), the associated precipitation composite indicates below normal precipitation over the SW and above normal precipitation over the PNW. The precipitation signal is the strongest when the enhanced convection is located at 120°E (Fig. 3a). In the Tropics, enhanced convection in the western Pacific is accompanied by suppressed convection in the central Pacific and over the Indian Ocean (Fig. 4a). Along the west coast of the United States, OLRAs are consistent with the observed precipitation composite (Fig. 3a). The precipitation anomalies are supported by the circulation anomalies (Fig. 5a). There is a quadrupole straddling the equator in the western Pacific and a wave train extending from the convective region passing through the North Pacific and the Gulf of Alaska to the western United States. The positive anomalies over the West Coast are not statistically significant at the 95% level, but they are consistent with the precipitation anomalies.

When the base box shifts from 120°E toward 150°E (Figs. 4a–c), the three-cell OLRA pattern in the Tropics shifts eastward. The cloud bands (negative OLRAs) located in the subtropics near 20°N extend northeastward toward California. The circulation anomalies show an eastward shift of the quadrupole along the equator. Negative anomalies in the Gulf of Alaska shift eastward to North America (Figs. 5a–c). The precipitation anomaly composites indicate a northward shift of dryness from California to the PNW (Figs. 3a–c).

When the base box is located at 150°E (Fig. 4c), the three-cell pattern in the Tropics is in quadrature with the OLRA pattern for the base box centered at 120°E (Fig. 4a). The streamfunction anomalies (Fig. 5c) in the Pacific–North American region are also nearly in quadrature with anomalies for the base box at 120°E (Fig. 5a). The cloud bands in the subtropics extend to the West Coast and California receives above normal pre-

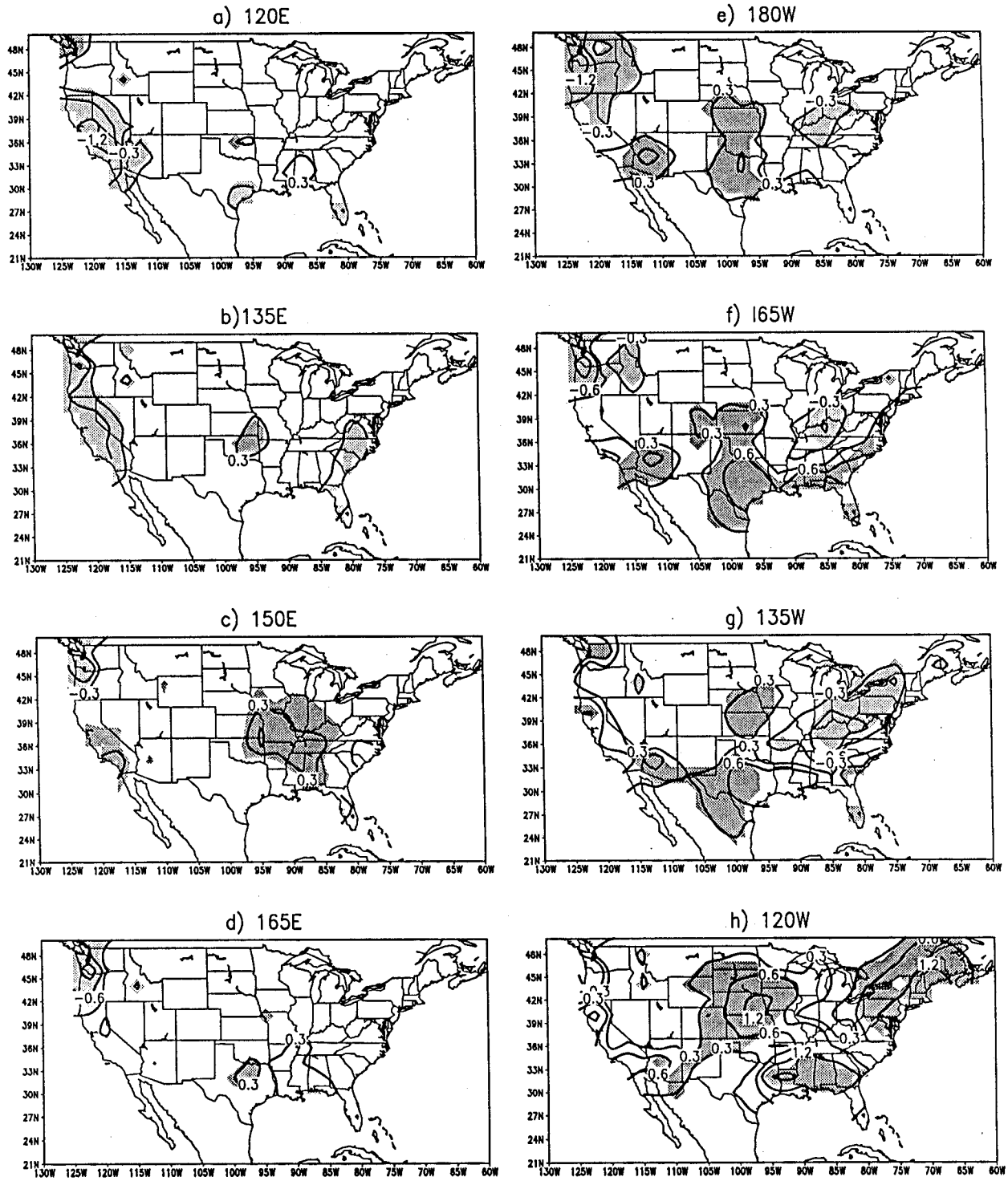

FIG. 3. Composite of observed precipitation anomalies based on the tropical OLRAs averaged over a 10° × 10° box centered at 5°S: (a) 120°E, (b) 135°E, (c) 150°E, (d) 165°E, (e) 180°, (f) 165°W, (g) 135°W, and (h) 120°W. Contour interval is 0.3 mm day^{-1}. Zero contours are omitted. Areas where positive (negative) values are statistically significant at the 95% are dark (light) shaded. See text for details.

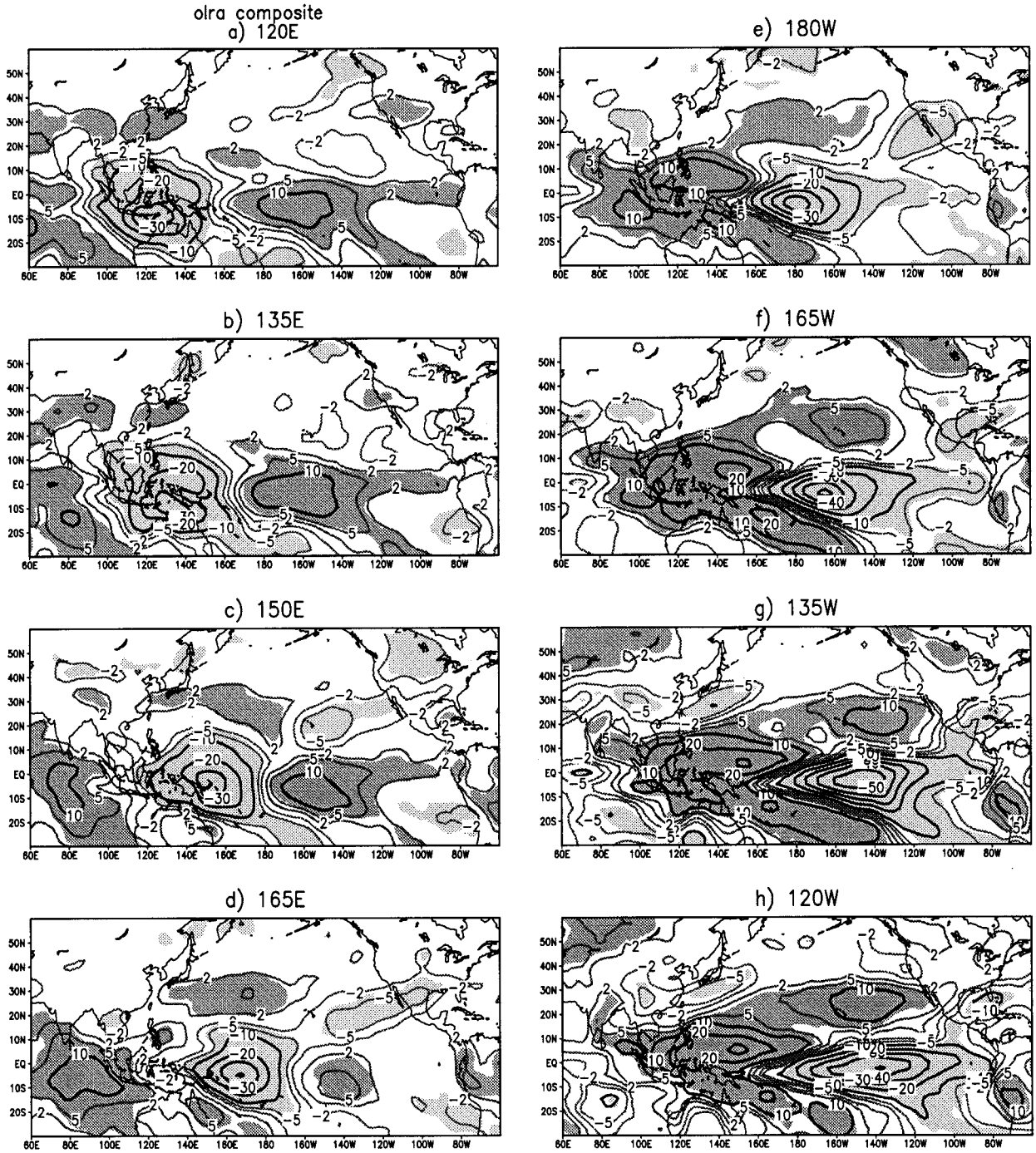

FIG. 4. Same as Fig. 3 but for composites of OLRAs. Contour interval is 10 W m^{-2}. Zero contours are omitted. Contours of −2, −5, 2, and 5 W m^{-2} are added. Areas where positive (negative) OLRA are statistically significant at the 95% level are dark (light) shaded.

cipitation while the PNW remains dry. The precipitation anomalies are out of phase with the precipitation anomalies for the base point at 120°E (Fig. 3c).

When the base box shifts from 150°E toward the date line, positive OLRAs shift from the Indian Ocean to the western Pacific while positive OLRAs in the eastern Pacific weaken and are confined to the area from the date line to 120°W (Figs. 4c,d). The cloud bands in the subtropics extend from the subtropical eastern Pacific to the Gulf of Mexico. The circulation anomalies (Figs. 5c,d) indicate the eastward shift of the anticyclonic couplet in the Tropics. In midlatitudes, there are no sig-

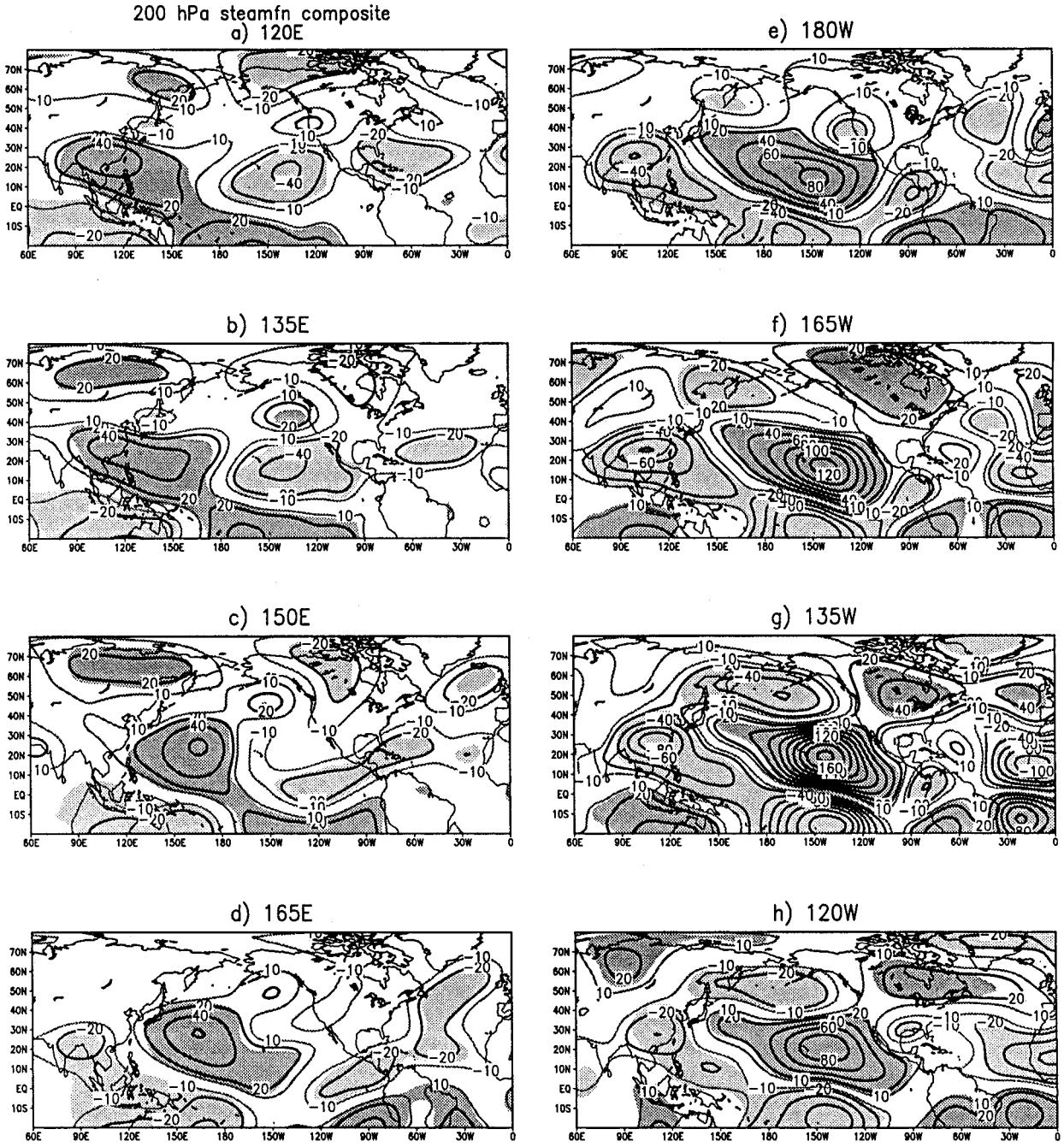

FIG. 5. Same as Fig. 3 but for composite of 200-hPa eddy–streamfunction anomalies. Contour interval is 20×10^5 m^2 s^{-1}. Zero contours are omitted. Contour intervals -10×10^5 m^2 s^{-1} and 10×10^5 m^2 s^{-1} are added. Areas where positive (negative) anomalies are statistically significant at the 95% level are dark (light) shaded.

nificant 200-hPa streamfunction anomalies in the North Pacific and over the United States for the base point at 165°E (Fig. 5d). The precipitation composite shows dryness over the PNW (Fig. 3d).

When the base box is centered at the date line, enhanced convection is located in the central and eastern Pacific with suppressed convection in the western Pacific (Fig. 4e). The enhanced local Hadley circulation strengthens and the subsidence is located in the subtropics near 25°–30°N. This enhanced upper-level convergence (positive OLRAs) extending from 160°E to 140°W prevents the formation of cloud bands. Therefore, the cloud bands shift eastward and extend to the Southwest and the Gulf of Mexico consistent with above

normal precipitation there (Fig. 3e), while the PNW remains dry.

When the base box is shifted to east of the date line (165°–135°W) (Figs. 4f,g), OLRAs in the Tropics show a dipole with enhanced convection in the central and eastern Pacific and suppressed convection in the western Pacific. The magnitudes of OLRAs are larger in comparison to composites based on boxes west of the date line. In the subtropics, positive OLRAs shift eastward to the subtropical eastern Pacific favoring wet conditions in the Southwest (Mo and Higgins 1998). In the Tropics, negative OLRAs extends from the eastern Pacific to the Gulf of Mexico. At 165°W, the cloud bands over the southern United States signal wet conditions (Fig. 3f). The rainband in the western region extends northward as the base boxes are shifted farther to the east. When the base box is located at 135°W, precipitation along the west coast and the southern United States is above normal (Fig. 3g).

The circulation responses are also stronger than responses when the base boxes are located west of the date line. The quadrupole with an anticyclonic pair centered east of the date line and a weaker cyclonic pair in the western Pacific shifts eastward with enhanced convection. The negative anomalies in the North Pacific and positive anomalies over the central and eastern United States shift eastward in concert (Figs. 5f,g). When the base point is located at 135°W, the circulation anomalies in the Western Hemisphere resemble a Pacific–North American teleconnection pattern (Wallace and Gutzler 1981). California receives most of its precipitation when positive OLRAs in the subtropical eastern Pacific reach a maximum.

When enhanced convection shifts farther eastward, the anticyclonic couplet in the central and eastern Pacific also moves eastward. When tropical heating is located at 120°W, negative 200-hPa streamfunction anomalies still cover the North Pacific. However, positive anomalies in the subtropics reach the west coast of California (Fig. 5h) with negative anomalies located over the Gulf of Mexico. There are no significant rainfall anomalies over the western region, but positive rainfall anomalies are found over the southern and central United States (Fig. 3h) and negative anomalies over the Ohio valley are found.

To summarize the response of precipitation anomalies in the western United States to tropical heating, we plotted precipitation anomalies averaged over the land points from 118° to 125°W at latitudes from 25° to 60°N (x axis) for base boxes from 90°E to 120°W (y axis) (Fig. 6a). We also show the corresponding OLRAs from 10° to 60°N for the same base boxes (Fig. 6b). Although OLR north of about 40°N may not be a good indicator of precipitation anomalies, it is included for completeness. When the base box is located in the western Pacific from 110° to 120°E, the PNW is wet and the SW is dry. The PNW receives below normal precipitation when enhanced tropical convection is located between 150°E and 150°W, while California receives above normal rainfall when tropical heating is located near 150°E or east of the date line consistent with the findings of Mo and Higgins (1998). This inverse relationship between precipitation anomalies in the SW and in the PNW exists when tropical convection is located 120°–150°E or from 180° to 150°W. These are the longitudes where OLRAs correspond well with precipitation anomalies over the United States. When tropical convection is located in those areas, there is also a phase reversal between cloud bands (negative OLRAs) in the subtropical eastern Pacific from 10° to 20°N and the precipitation anomalies in the SW (Fig. 6b). The precipitation anomaly patterns in the West are not very sensitive to the latitudinal locations of the tropical heating. When the base area is centered on 5°N or on the equator, the precipitation patterns in the West remain basically the same, but the magnitudes of the anomalies vary somewhat (Figs. 6c,d).

4. Contributions from the IS and IA bands

Next, we separate contributions from the IS and the IA bands. Figures 7 and 8 show the IS-filtered OLRAs and 200-hPa eddy–streamfunction composites for base boxes centered on 5°S, respectively. The contributions from the IA band are the differences between the composites for the total anomaly composites (Figs. 4 and 5) and composites for anomalies from the IS band. The IS-filtered OLRA patterns are similar to the total OLRAs but the magnitudes are weaker when base boxes are located west of the date line. The contributions to the OLRAs from the IS band are about 80% of the total anomalies in the Tropics and slightly more than 50% in the subtropics when tropical heating is located between 120°E and 165°W. This is the area where the tropical IO is the strongest (Lau and Chan 1985). When the base point is shifted to the east of 165°W, the tropical IO weakens and contributions are dominated from anomalies in the IA band.

When enhanced convection is located in the western Pacific, the convection pattern (Figs. 4a and 7a) can be found during cold ENSO events, but it is also a typical convection pattern associated with the tropical IO (Lau and Chan 1985). The patterns of the IS-filtered streamfunction composite and the total anomaly composite are similar (Figs. 5a and 8a). They both show negative anomalies over northern Alaska and positive anomalies near the west coast of California. These centers also appear in the 700-hPa height anomaly composite pattern associated with a positive SOI and above normal precipitation in the PNW (Cayan and Redmond 1994).

When the base box is shifted to 150°E (Fig. 7c), the OLRA pattern is in quadrature with the OLRA composite for the base box at 120°E (Fig. 7a) in the Tropics. The OLRA anomalies near California are negative. Results here agree with those reported by Mo and Higgins (1998) who found that wet (dry) episodes in California

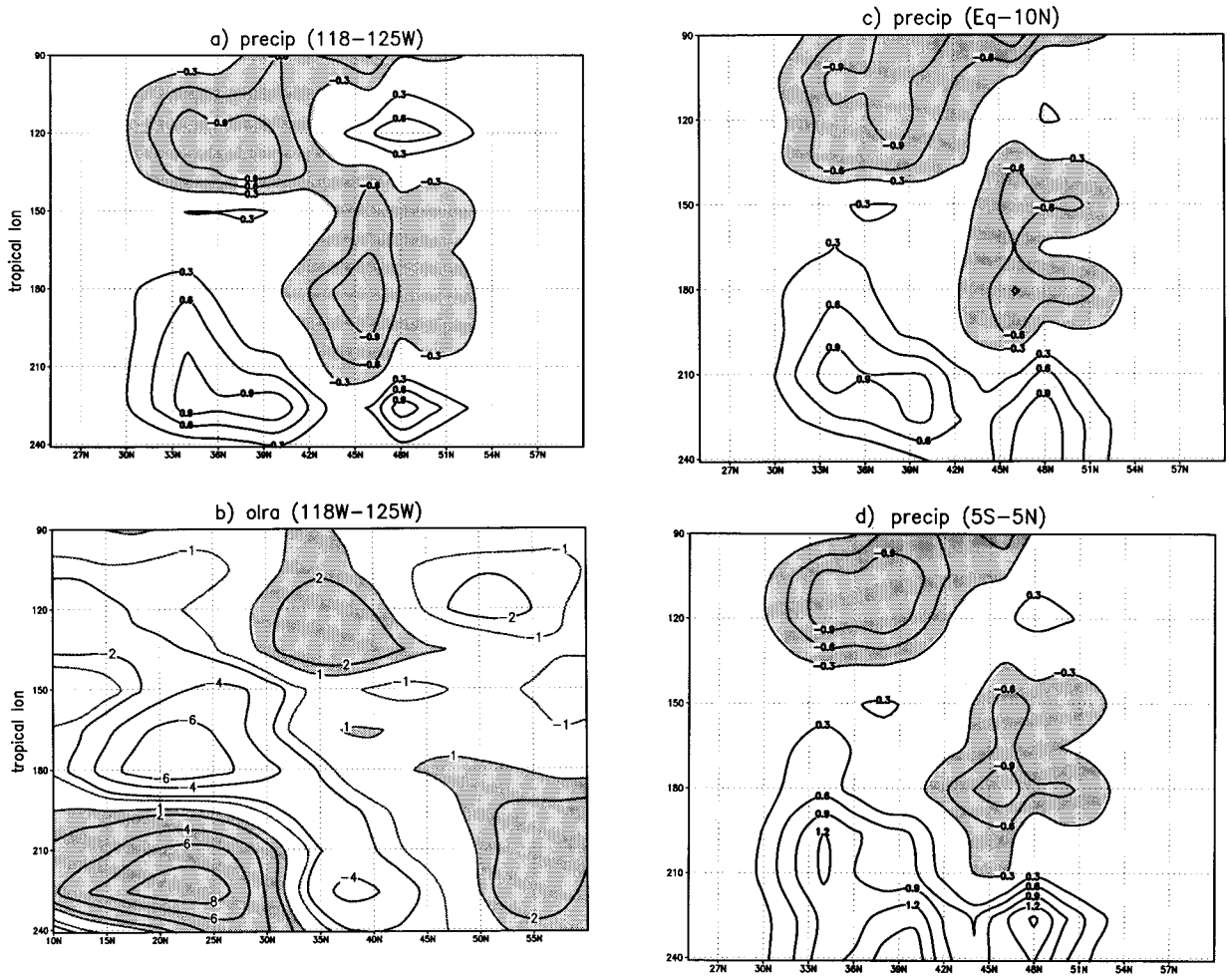

FIG. 6. (a) Observed precipitation anomaly composite averaged from 118° to 125°W for latitudes from 25° to 60°N (*x* axis) for the base boxes centered from 5°S, 90°E to 5°S, 120°W every 15° to the east (*y* axis). Contour interval is 0.3 mm day^{-1}. Zero contours are omitted. (b) Negative values are shaded as in (a) but for OLRA from 10° to 60°N. Contour interval is 2 W m^{-2}. Zero contours are omitted. Contours −1 and 1 W m^{-2} are added and positive values are shaded. (c) Same as (a) but for base points centered along 5°N. (d) Same as (a) but for base points centered along the equator.

are favored when enhanced convection associated with the tropical IO reaches 150°E (120°E).

As enhanced convection moves eastward, the wave train from the Tropics also shifts eastward. When the base box is shifted from 150°E to 165°W, positive anomalies shift from 140°E, 65°N, (Fig. 8c) to the Gulf of Alaska strengthening (Figs. 8c–f), while negative anomalies shift from northern Alaska to the California coast. When enhanced convection reaches the date line, a Pacific–North American teleconnection pattern forms (Fig. 8e). The responses of the circulation anomalies and precipitation regimes to enhanced OLRAs west of the date line are very different from the responses due to heating east of the date line. When the base point is located east of 165°W, wet conditions generally prevail in the Southwest. Most contributions are from warm ENSO events in the IA band. The streamfunction responses (Figs. 5e–g) resemble 700-hPa height anomalies with a negative SOI and heavy precipitation in the Southwest given by Cayan and Redmond (1994).

5. Lagged responses

To examine lagged precipitation responses to tropical convection, we form composites of precipitation, 200-hPa eddy–streamfuncion, and OLR anomalies from day 1 to day 25 after OLRA averaged over the base box in the Tropics was found to be below −0.8 standard deviations. The base boxes are shifted along 5°S from 90°E to 120°W, as before.

When the base points are located west of the date line, the OLRA composites show a mixed standing and eastward propagating characteristics of tropical convection similar to those reported by Kiladis and Weickmann (1992a). Figures 9a–c show the time–latitude diagrams of the rainfall anomalies averaged over land points from

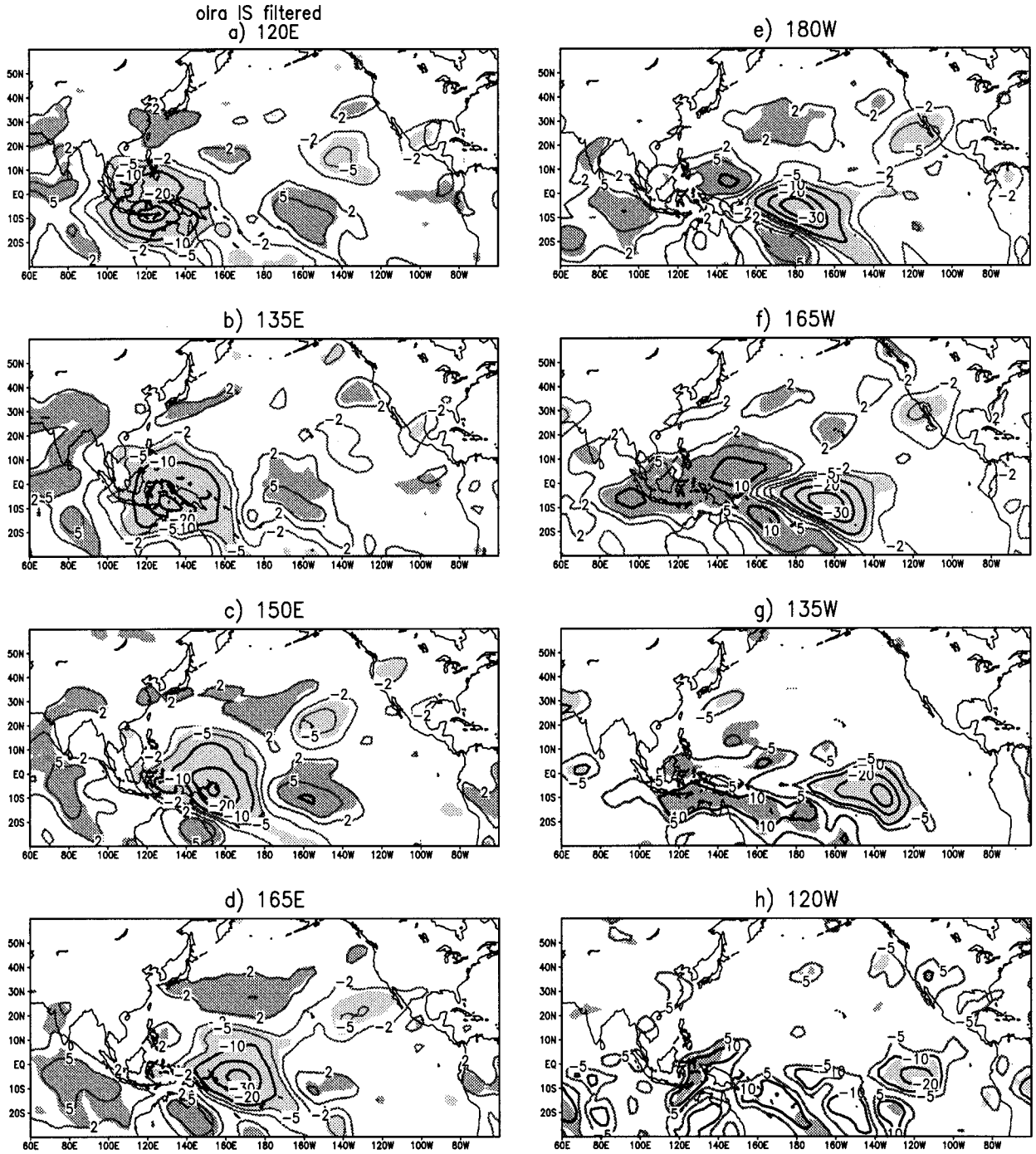

FIG. 7. Same as Fig. 4 but for IS-(10–90 day) filtered OLRA.

118° to 125°W at selected base points while the corresponding time–longitude diagrams for OLRAs averaged from 10°S to the equator are given in Figs. 9d–f. When the base point is located at 90°E in the Indian Ocean, the response in rainfall is only significant at the 90% level. The OLRA move eastward as indicated by the three-cell pattern in the Tropics. Negative OLRAs reach 120°E at day 6 and rainfall anomalies start to become significant at the 95% level. Figure 9a shows rainfall deficit in California (32°–42°N). After day 6, OLRAs continue to propagate eastward and the precipitation anomalies persist until day 20.

When the base point is located at 120°E, the associated precipitation pattern shows dryness in the SW and wetness in the PNW (Fig. 3a). As the time progresses, tropical convection propagates eastward. There

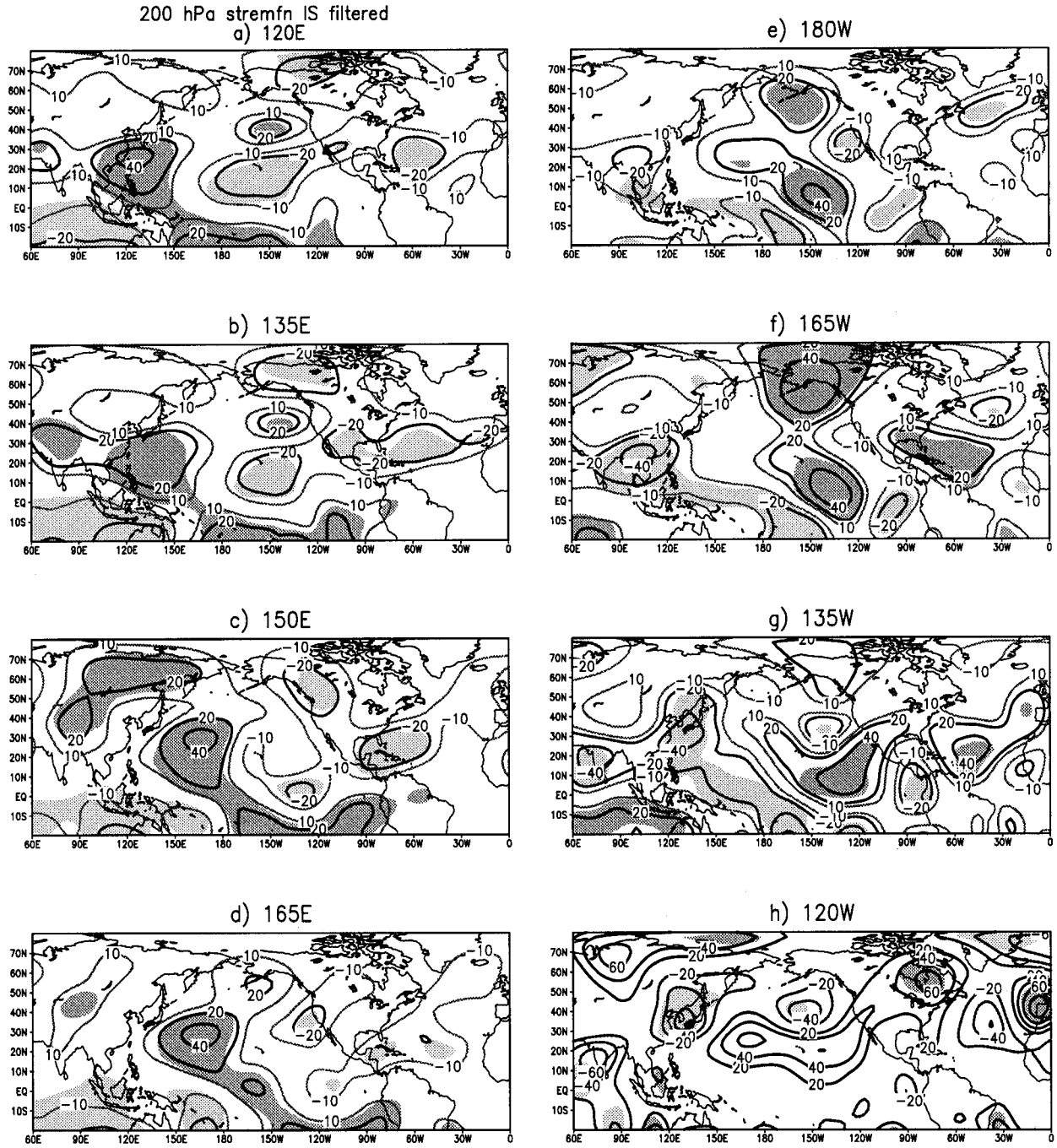

FIG. 8. Same as Fig. 5 but for IS-(10–90 day) filtered 200-hPa eddy–streamfunction.

is a northward shift of dryness during the first 6 days (Fig. 9b). In the Tropics, the three-cell OLRA pattern moves eastward. At day 6, the convection extends to 160°E, and the 200-hPa streamfunction anomaly map (not shown) resembles the 200-hPa height anomaly response to OLRAs at 120°E in the 30–60–day band (Kiladis and Weickmann 1992a, their Fig. 6b), which shows intensification and eastward extension of positive anomalies along the west coast of North America, consistent with the dryness in the PNW. After day 6, OLRAs continue to move eastward, weakening, and the associated precipitation anomalies persists through day 20.

When the base point is located at 150°E, the precipitation anomalies show wetness in the SW and dryness in the PNW (Fig. 3c). When convection moves away from 150°E and toward the date line, dryness in the PNW persists. At day 10, negative OLRAs reach the date line and positive precipitation anomalies appear in

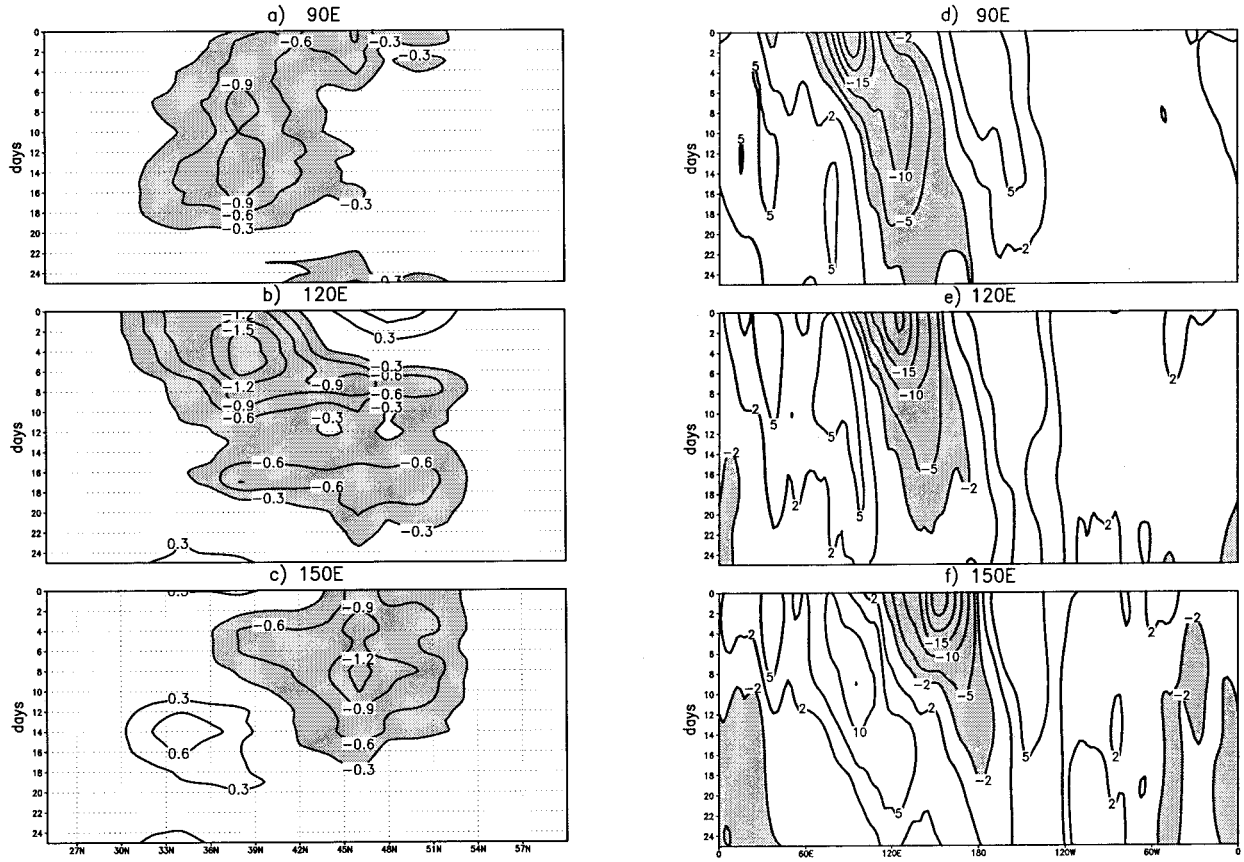

FIG. 9. Precipitation anomaly composite averaged from 118° to 125°W for latitudes from 25° to 60°N (*x* axis) from day 0 to day 25 for the base boxes centered at (a) 5°S, 90°E, (b) 5°S, 120°E, and (c) 5°S, 150°E. Contour interval is 0.3 mm day^{-1}. Zero contours are omitted. Negative values are shaded, and the time–longitude diagram for OLRA averaged from 10°S to the equator for the base point at (d) 5°S, 90°E, (e) 5°S, 120°E, and (f) 5°S, 150°E. Contour interval is 5 W m^{-2}. Contours −2 and 2 W m^{-2} are added.

the SW while negative rainfall anomalies persist in the PNW.

When the base boxes are located east of the date line, most contributions are from the IA band. The convection persists for about 15 days and weakens gradually. The associated precipitation anomaly pattern (not shown) is similar to the simultaneous response for the same base point (Fig. 3). The pattern stays the same for 15 days and the magnitudes of the anomalies vary according to the strength of the OLRAs.

6. Physical mechanisms

a. Zonal wind and eddy kinetic energy

Both Mo and Higgins (1998) and Dettinger et al. (1998) recognized the importance of relationships between zonal wind anomalies and precipitation regimes in the United States. They both indicated that above (below) normal precipitation in California is associated with the eastward extension (retraction) of the Pacific subtropical jet. Figure 10 shows composites of the 200-hPa zonal wind (shaded) and anomaly composites keyed to tropical OLRAs in various base boxes. The zonal wind anomalies averaged over 150°–120°W keyed to OLRAs from 90°E to 120°W at 5°S are given in Fig. 11a. They are consistent with 200-hPa streamfunction anomalies (Fig. 5). The storm track represented by the 200-hPa bandpass-filtered (2.5–6 day) kinetic energy anomalies averaged over the same longitude band is given in Fig. 11b.

In general, the subtropical jet is located west of 150°W, when enhanced convection is located in the western Pacific or over the Indian Ocean. However, local wind anomalies depend on the details of the tropical heating pattern. When the base box is located between 120° and 135°E, the jet stream over North America shifts northward as indicated by the dipole of zonal wind anomalies (Figs. 10a, 10b, and 11a). The northward shift of the upper-level zonal wind is accompanied by the northward shift of synoptic-scale eddies indicated by positive anomalies of the bandpass-filtered kinetic energy anomalies (Fig. 11b). This is consistent with above normal precipitation in the PNW and below normal precipitation in the SW.

When the base point shifts eastward, the Pacific jet shifts eastward and connects with the North American

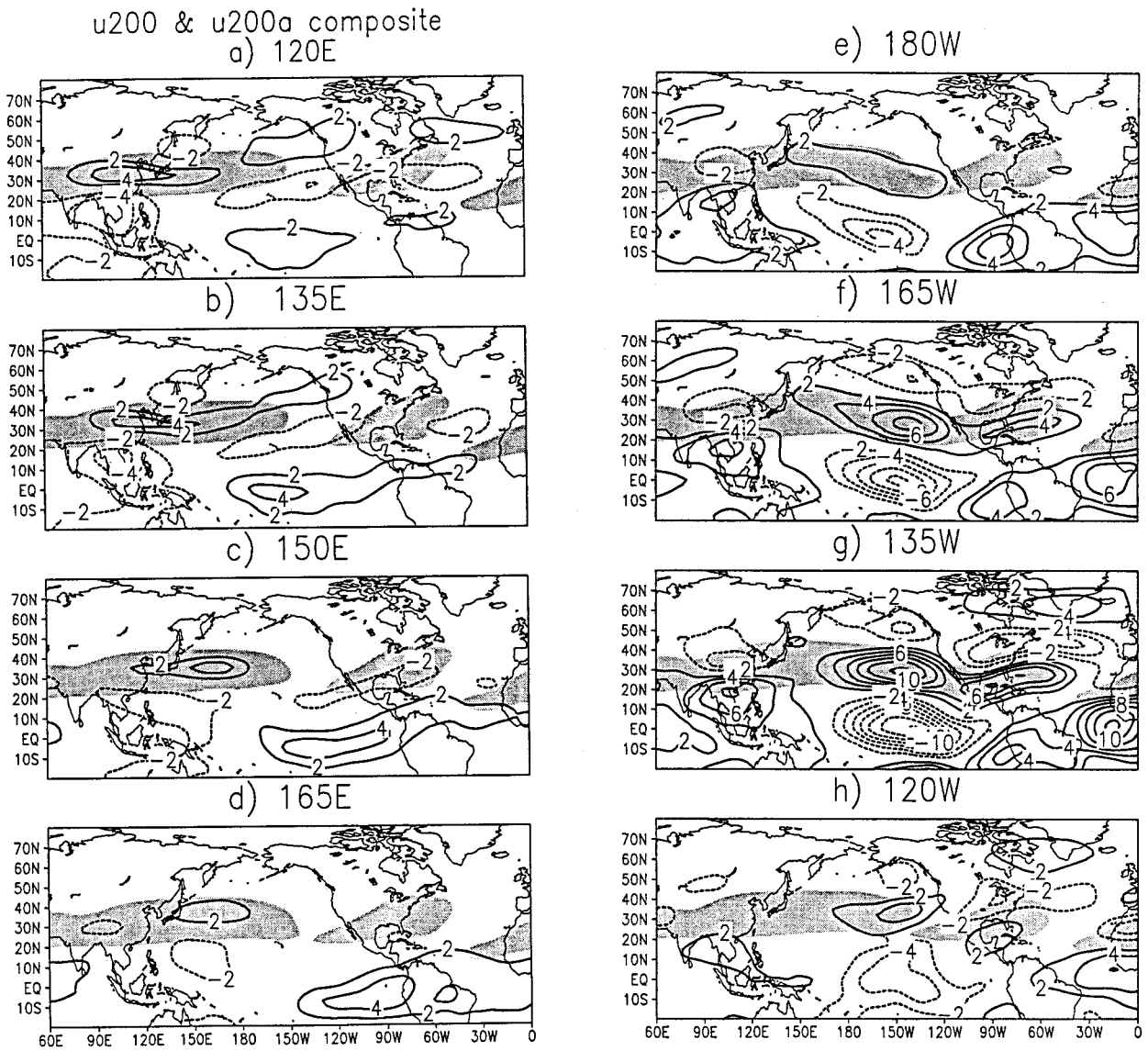

FIG. 10. Same as Fig. 4 but for composite of 200-hPa zonal wind (shaded) and wind anomalies (contoured). Zonal winds greater than 30 m s^{-1} are shaded. Zero contours are omitted. Contour interval for zonal wind anomaly is 2 m s^{-1}.

jet (Figs. 10d–g). When the base box is located between 165° and 135°W, the westerlies over California reach maximum values. The storm track also shifts southward (Fig. 11b) and precipitation increases in the SW. When the base box shifts to 120°W, westerlies decrease and precipitation over the SW also decreases. When the base box is located east of 165°W, most contributions are from the IA band, and both zonal wind anomalies and OLRA are stronger.

b. Rossby vorticity source

Shifts of the jet stream are related to tropical heating. This physical mechanism can be illustrated using 200-hPa S anomalies in the subtropics. A similar mechanism has been used to explain the shift of the jet stream during the 1987–89 ENSO cycle by Rasmusson and Mo (1993). Two examples are given for base boxes centered at 5°S, 135°E and 5°S, 135°W.

For the 5°S, 135°E case, enhanced divergence at 200-hPa (enhanced convection, dark shading) is located in the western Pacific and suppressed divergence (suppressed convection, light shading) is located in the central Pacific (Fig. 12b). In the subtropics, the subsidence of the local Hadley circulation is located along roughly 32°N as indicated by the divergent wind anomalies extending from the Tropics to the North Pacific. The enhanced convergence (light shading) located from 100° to 140°E in the midlatitudes and suppressed convergence (dark shading) located from 160°E to 160°W are

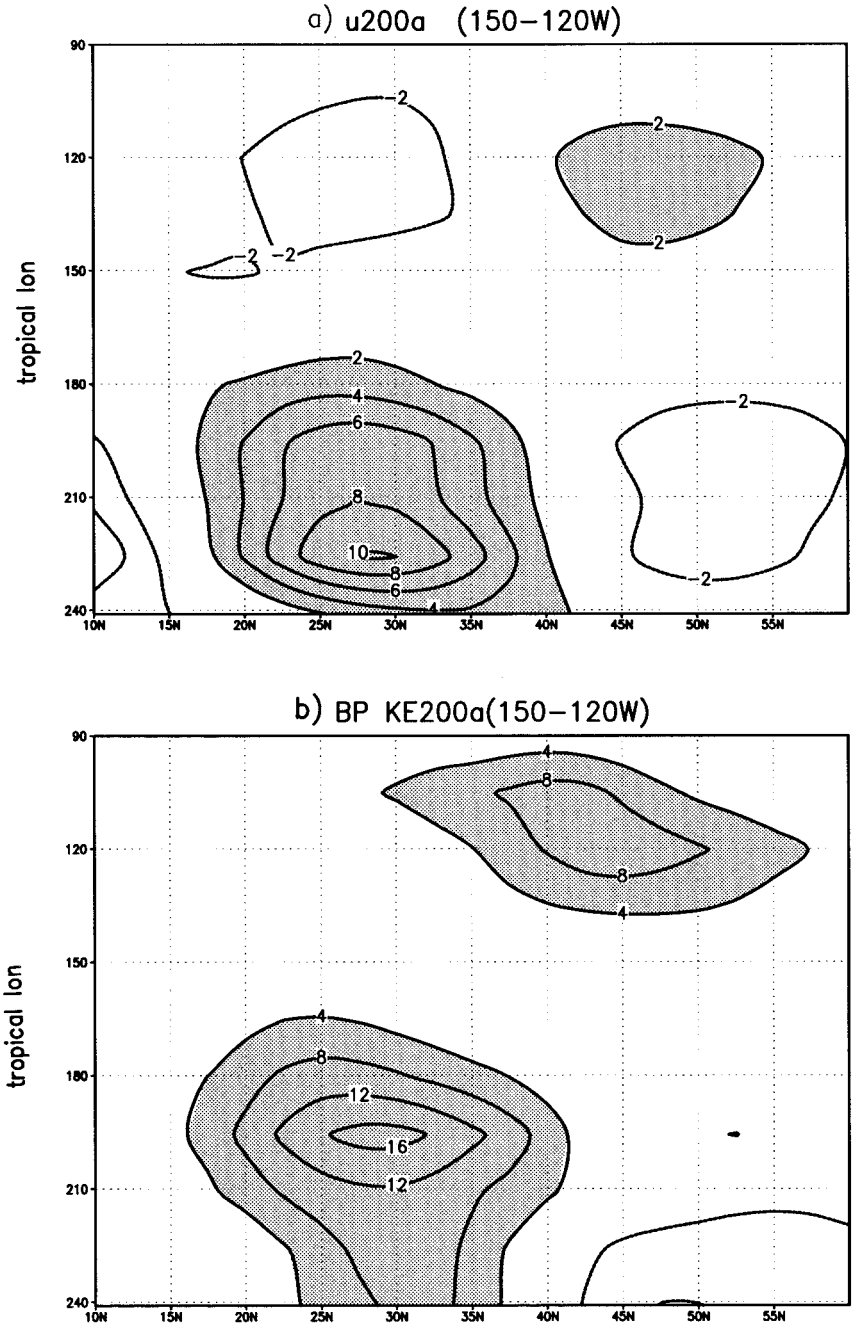

FIG. 11. Same as Fig. 4b but for (a) 200-hPa zonal wind anomaly composites averaged from 120° to 150°W. Contour interval is 2 m s^{-1}. Zero contours are omitted and positive values are shaded. (b) Same as (a) but for 200-hPa bandpass-filtered kinetic energy anomaly composites averaged from 120° to 150°W. Contour interval is 4 $(m\ s^{-1})^2$. Zero contours are omitted and positive values are shaded.

related to the local Hadley circulation. The enhanced convergence is located southeast of the positive *S* anomalies centered at 125°E and the suppressed convergence corresponds to negative *S* anomalies in the North Pacific centered near 170°E (Fig. 12a). The negative *S* anomalies in the North Pacific discourage the eastward extension of the Pacific subtropical jet and positive *S* anomalies strengthen the jet in the western Pacific (Fig. 10b).

For the 5°S, 135°W case, the enhanced divergence

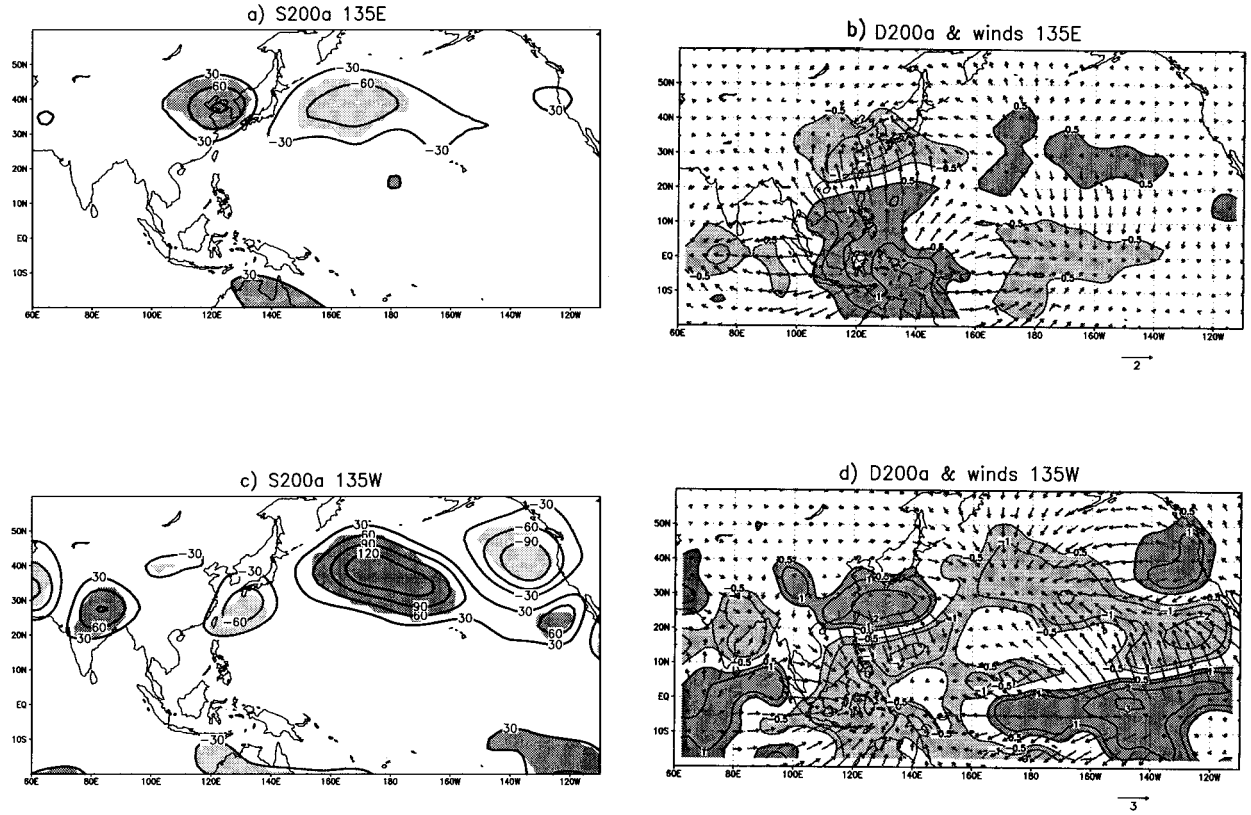

FIG. 12. (a) Composite of 200-hPa S anomalies based on the tropical OLRA averaged over a 10° × 10° box centered at 5°S, 135°E. Contour interval is 30 × 10^{-12} s^{-2}. Zero contours are omitted. (b) Divergence (contours) and divergent wind (arrow) anomalies. Values greater than 0.5 × 10^{-6} s^{-1} are dark shaded and values less than −0.5 × 10^{-6} s^{-1} are light shaded. Unit for wind anomaly is 2 m s^{-1}. (c) Same as (a) but for box at 5°S, 135°W, (d) Same as (b) but for the base box at 5°S, 135°W. Unit for wind anomaly is 3 m s^{-1}.

(dark shading) in the Tropics extending from 170°E to 120°W (Fig. 12d) creates anomalous positive *S* (Fig. 12c) extending from the date line at 40°N southeastward to the California coast near 120°W, where zonal wind anomalies (Fig. 10g) are positive. Therefore, tropical heating in the subtropical eastern Pacific is at least partially responsible for moving the upper-level zonal winds toward California.

7. Summary and discussion

This study uses a multiyear daily precipitation dataset and the NCEP–NCAR reanalysis data to document the relationship between locations of tropical convection and precipitation regimes in the western United States. The daily data allow us to study precipitation regimes associated with tropical convection at timescales less than 1 month and contributions from IA and IS bands may be discussed separately. Circulation patterns associated with precipitation regimes were examined. Attempts were made to examine tropical–extratropical linkages using the one-level vorticity balance equation. The responses of the precipitation anomalies over the western region of the United States can be summed up according to the locations of the tropical convection.

a. Tropical convection in the western Pacific

Enhanced convection in the western Pacific favors dry conditions in the SW and wet conditions in the PNW. Fluctuations in both the IS and the IA bands contribute to this variability. Enhanced convection in the western Pacific is accompanied by suppressed convection in the central Pacific. The Hadley cell strengthens in the western Pacific and weakens in the central Pacific. The associated positive S anomalies in the subtropics at 35°N, 120°E and negative anomalies in the North Pacific are at least partially responsible for a retracted Pacific jet west of 150°W. The storm track follows the jet and moves to the North Pacific so that the Southwest receives below normal precipitation.

b. Tropical convection located from 150°E to the date line

When the tropical convection is located west of the date line, substantial contributions to OLRA are from

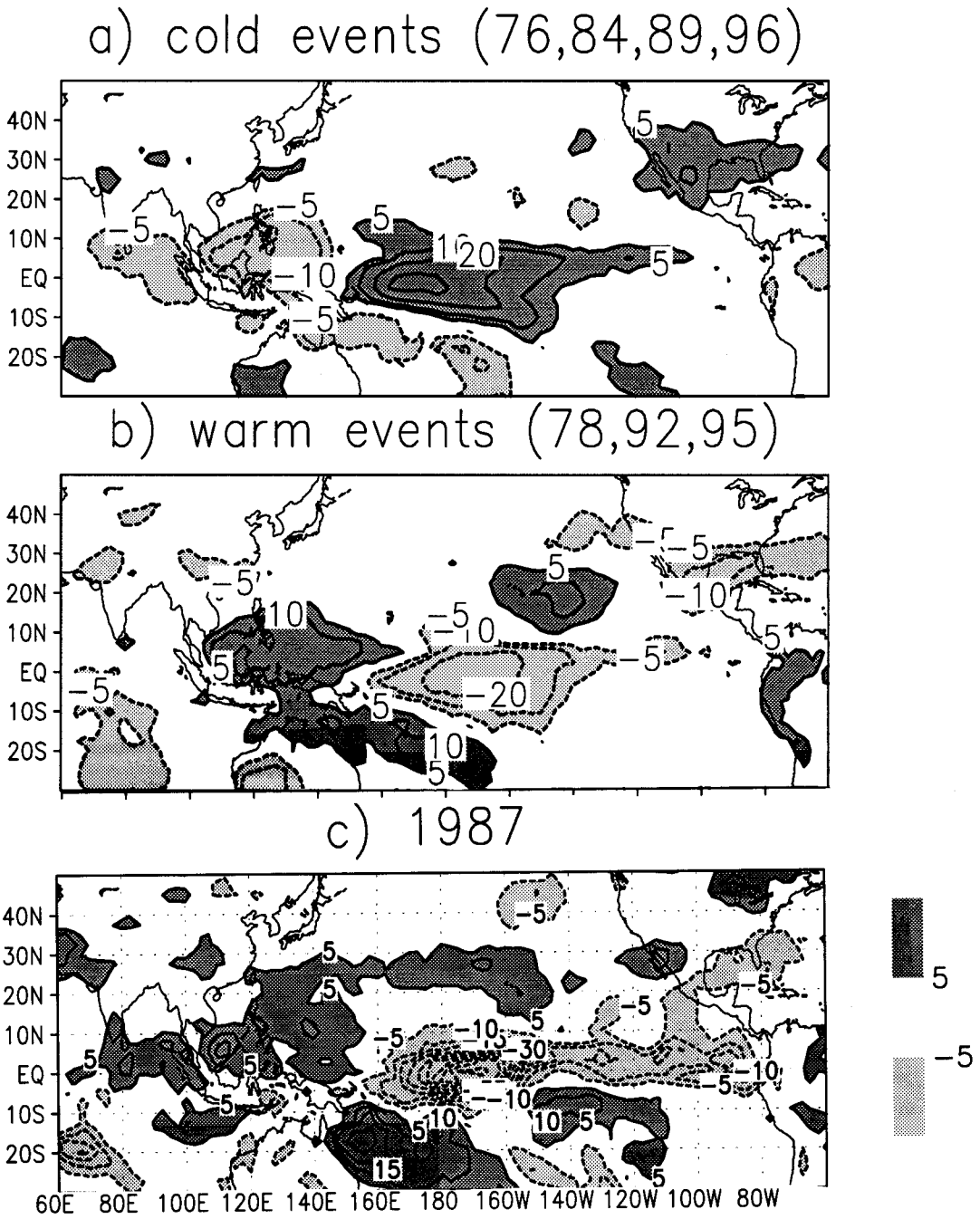

FIG. 13. Mean winter OLRA averaged over (a) cold events (1976, 1984, 1989, and 1996), (b) warm events (1978, 1992, and 1995), and (c) winter mean OLRA for 1987. Contour interval is 10 W m^{-2}. Zero contours are omitted and contours 5 and −5 W m^{-2} are added. Positive (negative) values are dark (light) shaded.

fluctuations in the IS band. When negative OLRAs are centered at 150°E, the SW receives above normal rainfall and the PNW is dry. When convection moves away from 150°E, the PNW remains dry while California has near normal rainfall The wave train extends from the convective area to North America where the 200-hPa streamfunction anomalies are consistent with the precipitation regimes.

c. Tropical convection in the central Pacific

When enhanced convection is located east of 165°W, most contributions are mainly from the IA band. The convection pattern is more persistent and the responses are stronger. When tropical convection is enhanced in the central Pacific from the date line to 135°W, the subsidence of the enhanced local Hadley circulation is lo-

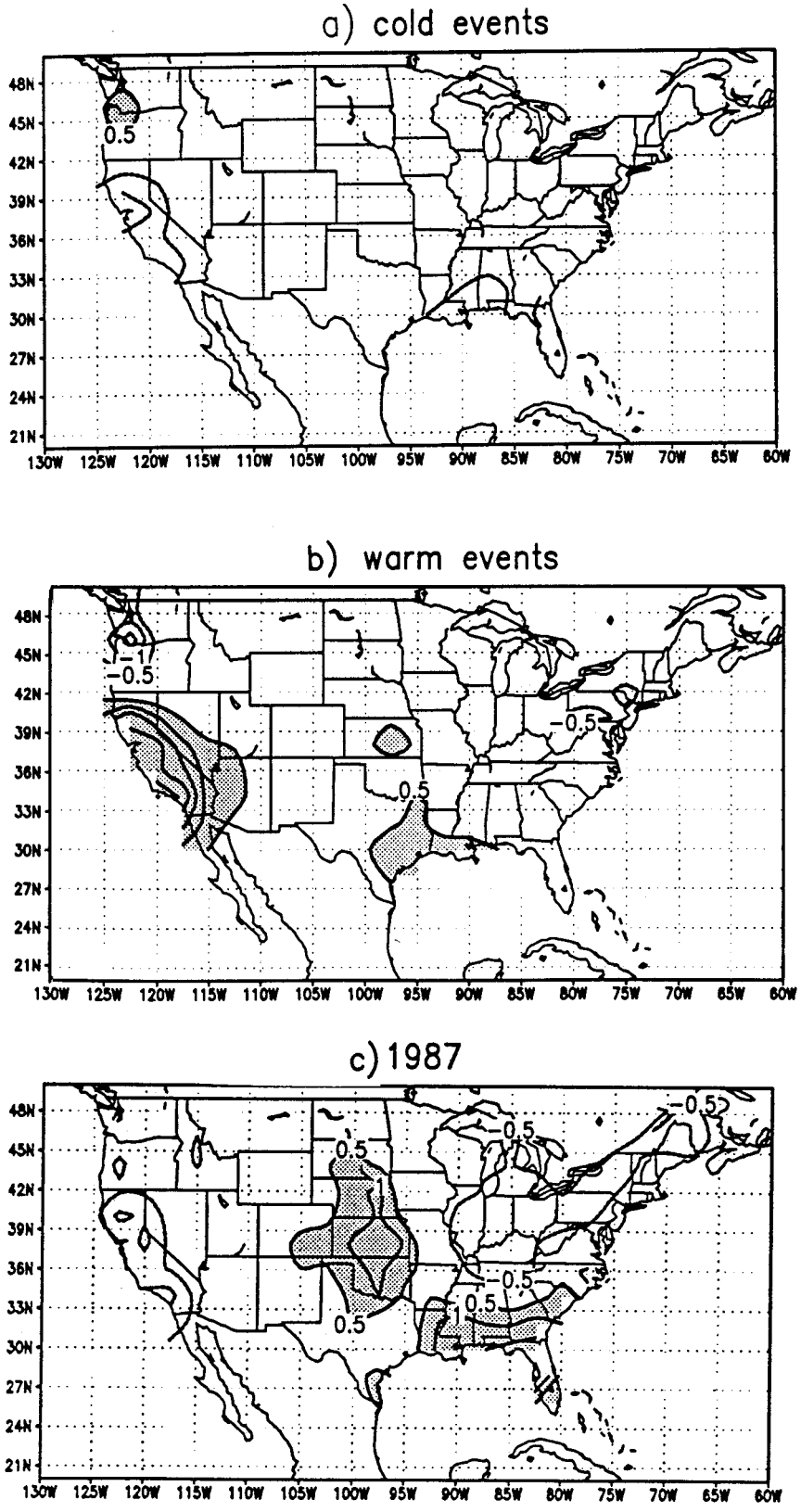

FIG. 14. Same as Fig. 13 but for winter mean precipitation anomalies. Contour interval is 0.5 mm day^{-1}. Zero contours are omitted and positive values are shaded.

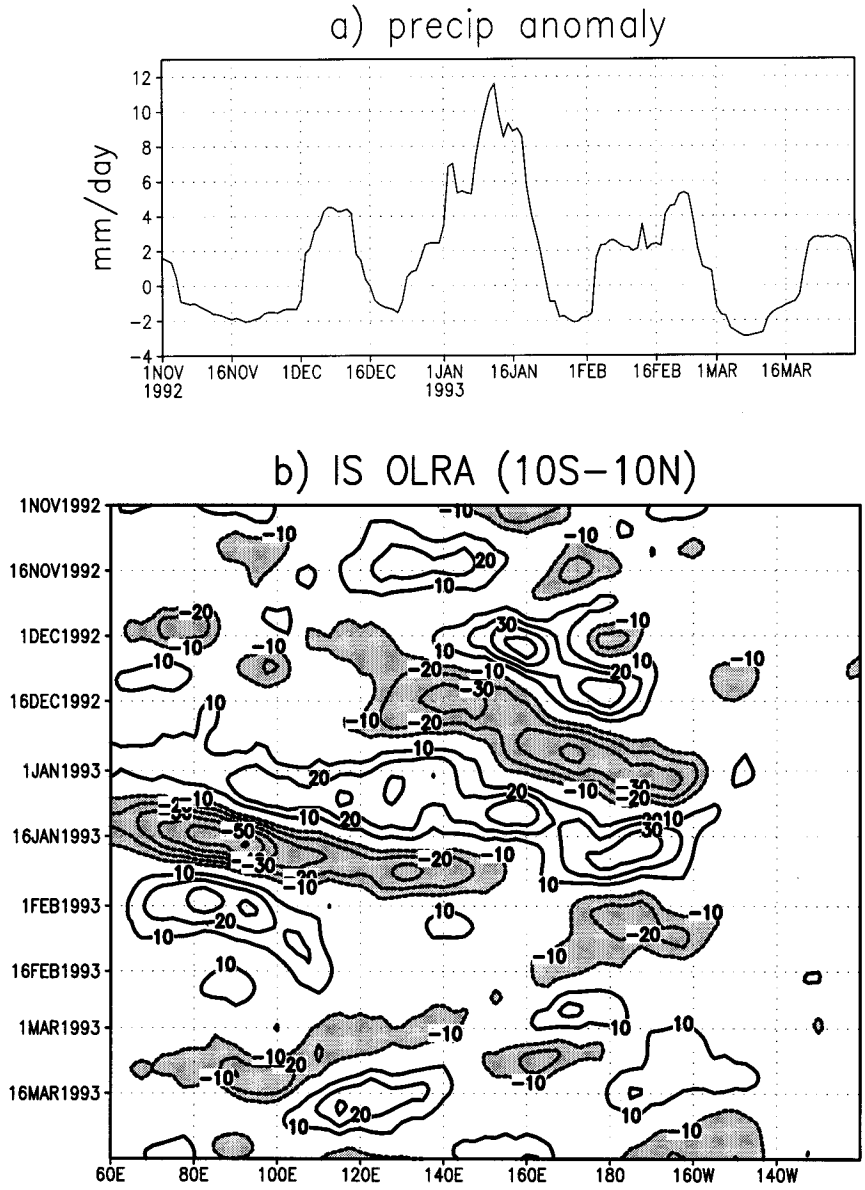

FIG. 15. (a) 10-day running mean observed daily precipitation mean anomalies averaged over Southern California (32°–38°N, 118°–125°W). The unit is mm day^{-1}. (b) Time–longitude plot for 10-day running mean IS-filtered OLRA averaged from 10°S to 10°N. Contour interval is 10 W m^{-2}. Zero contours are omitted. Negative values are shaded.

cated in the subtropical eastern Pacific. This configuration creates positive *S* anomalies from the North Pacific to the west coast near California. Enhanced *S* anomalies are at least partially responsible for the eastward shift of the subtropical jet. The storm track also moves southward, consistent with wet conditions in the Southwest and dry conditions in the PNW.

d. Tropical convection in the eastern Pacific

When the maximum tropical heating is located near 135°W, the northward shift of the rainband brings heavy precipitation to the entire western region. If enhanced convection occurs in the eastern Pacific east of 120°W in addition to heating in the central Pacific, convergence (positive OLRA) extends from the subtropical eastern Pacific to the southern United States consistent with above normal rainfall there, while the SW has near normal rainfall.

The above results can be applied to explain precipitation regimes during ENSO events. For the period that the OLR records are available, there were four cold ENSO events (1976, 1984, 1989, and 1996). We included the 1984 event because cold sea surface tem-

perature anomalies (SSTA) were located in the central Pacific. The OLRAs averaged over the four winters show a convection pattern (Fig. 13a) similar to the pattern keyed to OLRA at 120°E (Fig. 4a), which favors below normal rainfall in the Southwest and above normal precipitation in the PNW (Fig. 3a). This is consistent with the precipitation anomalies averaged over the same cold events (Fig. 14a).

During this period, there were three warm events (1978, 1992, and 1995) showing above normal rainfall in the SW and dryness in the PNW (Fig. 14b). The corresponding OLRA (Fig. 13b) and precipitation anomaly pattern (Fig. 14b) are similar to the patterns keyed to OLRA at 165°W (Figs. 3g and 4g). Figure 13b also resembles the OLRAs pattern for the type 1 ENSO events defined by Fu et al. (1986). These ENSO events have SST warming in the central and eastern Pacific and near normal conditions in the western Pacific and have been linked to wetness in the Southwest and dryness in the PNW (Schonher and Nicholson 1989; Cayan and Webb 1992; Kahya and Dracup 1994).

The 1987 warm event shows below normal precipitation in the Southwest (Fig. 14c). The winter mean OLRAs for 1987 (Fig. 13c) indicates enhanced convection centered near 165°W with a second OLRAs minimum located near 90°W. The OLRAs composite with the base point at 90°W (not shown) is similar to that at 120°W (Fig. 4h). Cloud bands extend farther eastward to Florida and positive OLRAs are located over California, consistent with dryness in California (Fig. 13c) and wetness over Florida.

The precipitation regimes are also modulated by the tropical IO. An example is given in Fig. 15. The mean precipitation anomaly over (118°–125°W, 32°–38°N) indicates four rainfall episodes in California during the 1992/93 winter (Fig. 15a). This corresponds well with four episodes of the tropical IO (Fig. 15b). The first episode started in November and enhanced convection reached the date line around 1 December 1992 while rain started in California. When enhanced convection moved out to the central Pacific, it reappeared over the Indian Ocean. Negative OLRAs associated with the second episode reached the central Pacific in late December and precipitation in California increased subsequently. The third episode started around 16 January 1993 in the Indian ocean. When enhanced convection reached the western Pacific, rainfall in California reached a minimum, and rainfall increased when negative OLRAs reached the central Pacific. The final episode in March was weaker and less regular, but the correspondence between precipitation in California and enhanced convection in the central Pacific is still very good

In this paper, we concentrated on tropical heating in the Pacific sector. We have not considered the effect of heating sources in Central America and/or in the Atlantic. There are also cases where precipitation in the western region is influenced by SSTA in the North Pacific (Masutani and Mo 1995). We have not considered the feedback of midlatitude anomalies to tropical convection as noted by Kiladis and Weickmann (1992b) and Liebmann and Hartmann (1984). These are topics for future work. This paper is diagnostic in nature. While it is clear that precipitation in the western United States is related to tropical convection, the total precipitation variance directly attributable to tropical OLRA is about 20%. More work is needed to apply findings here to real-time forecasting.

REFERENCES

Berbery, E. H., and J. N. Paegle, 1993: Intraseasonal interactions between the tropics and extratropics in the Southern Hemisphere. *J. Atmos. Sci.,* **50,** 1950–1965.

Blackmon, M. L., 1976: A climatological spectral study of the 500-mb height of the Northern Hemisphere. *J. Atmos. Sci.,* **33,** 1607–1623.

Cayan, D. R., and D. H. Peterson, 1989: The influence of north Pacific atmospheric circulation on streamflow in the west. *PACLIM, Geophys. Monogr.,* No. 55, Amer. Geophys. Union, 375–397.

——, and R. H. Webb, 1992: El Nino–Southern Oscillation and streamflow in the western United States. *Historical and Paleoclimatic Aspects of the Southern Oscillation,* H. F. Diaz and V. Markgraf, Eds., Cambridge University Press, 29–68.

——, and K. T. Redmond, 1994: ENSO influences on atmospheric circulation and precipitation in the western United States. *Proc. Tenth Annual Pacific Climate (PACLIM) Workshop,* Asilomar, CA, California Department of Water Resources, 5–26.

Dettinger, M. D., D. R. Cayan, H. F. Diaz, and D. M. Meko, 1998: North–south precipitation patterns in western North America on interannual-to-decadal timescales. *J. Climate,* in press.

Fu, C., H. F. Diaz, and J. O. Fletcher, 1986: Characteristics of the response of SST in the central Pacific associated with warm episodes of the Southern Oscillation. *Mon. Wea. Rev.,* **114,** 1716–1738.

Higgins, R. W., and K. C. Mo, 1997: Persistent North Pacific circulation anomalies and the tropical intraseasonal oscillation. *J. Climate,* **10,** 223–244.

——, J. E. Janowiak, and Y. P. Yao, 1996: A gridded hourly precipitation data base for the United States (1963–1993). *NCEP/Climate Prediction Center Atlas No. 1,* NCEP/NWS/NOAA, 47 pp.

Kahya, E., and J. A. Dracup, 1994: The influences of type 1 El Niño and La Niña events on streamflows in the Pacific southwest of the United States. *J. Climate,* **7,** 965–976.

Kalnay, E., and Coauthors, 1996: The NCEP–NCAR 40-year reanalysis project. *Bull. Amer. Meteor. Soc.,* **77,** 437–471.

Kiladis, G. N., and K. M. Weickmann, 1992a: Circulation anomalies associated with tropical convection during northern winter. *Mon. Wea. Rev.,* **120,** 1900–1923.

——, and ——, 1992b: Extratropical forcing of tropical Pacific convection during northern winter. *Mon. Wea. Rev.,* **120,** 1924–1938.

Lanzante, J. R., and R. P. Harnack, 1982: Specification of United States summer season precipitation. *Mon. Wea. Rev.,* **110,** 1843–1850.

Lau, K. M., and P. H. Chan, 1985: Aspects of the 40–50 day oscillation during the northern winter as inferred from outgoing longwave radiation. *Mon. Wea. Rev,* **113,** 1889–1909.

Liebmann, B., and D. L. Hartmann, 1984: An observational study of tropical–midlatitude interaction on intraseasonal time scales during winter. *J. Atmos. Sci.,* **41,** 3333–3350.

——, and C. A. Smith, 1996: Description of a complete (interpolated) outgoing longwave radiation dataset. *Bull. Amer. Meteor. Soc.,* **77,** 1275–1277.

Masutani, M., and K. C. Mo, 1995: Physical mechanisms for the 1995 California floods. *Proc. 20th Annual Climate Diagnostics Workshop,* Seattle, WA, Climate Prediction Center/NCEP, 13–16.

Mo, K. C., and R. W. Higgins, 1998: Tropical influences on California precipitation. *J. Climate*, **11,** 412–430.

Papoulis, A., 1973: Minimum bias windows for high resolution spectral estimates. *IEEE Trans. Inf. Theory*, **19,** 9–12.

Rasmusson, E. M., and K. C. Mo, 1993: Linkages between 200-mb tropical and extratropical circulation anomalies during the 1986–1989 ENSO cycle. *J. Climate*, **6,** 595–616.

Redmond, K. T., and D. R. Cayan, 1994: El Nino–Southern Oscillation and western climate variability. Preprints, *Sixth Conf. on Climate Variations*, Nashville, TN, Amer. Meteor. Soc., 141–145.

Richman, M. B., and P. J. Lamb, 1985: Climatic pattern analysis of three- and seven-day summer rainfall in the central United States: Some methodological considerations and a regionalization. *J. Climate Appl. Meteor.*, **24,** 1325–1343.

Sardeshmukh, P. D., and B. J. Hoskins, 1988: The generation of global rotational flow by steady idealized tropical divergence. *J. Atmos. Sci.*, **45,** 1228–1251.

Schonher, T., and S. E. Nicholson, 1989: The relationship between California rainfall and ENSO events. *J. Climate*, **2,** 1258–1269.

Wallace, J. M., and D. S. Gutzler, 1981: Teleconnections in the geopotential height field during the Northern Hemisphere winter. *Mon. Wea. Rev.*, **109,** 784–812.